

Phase diagram of the betaine arsenate–betaine phosphate mixed-crystal system by dielectric hysteresis and current curves

S. Lanceros-Méndez

Departamento de Física, Universidade do Minho, 4710-057 Braga, Portugal

M. Köhler and G. Schaack

Physikalisches Institut der Universität Würzburg, Am Hubland, D-97074 Würzburg, Germany

A. Klöpperpieper

Fachbereich Physik der Universität des Saarlandes, D-66123 Saarbrücken, Germany

(Received 8 February 2006; published 31 May 2006)

The ferroelectric (FE) betaine arsenate (BA) and the antiferroelectric (AF) betaine phosphate (BP) are structurally very closely related and mixed crystals of $\text{BA}_x\text{BP}_{1-x}$ can be grown over the whole concentration range. The concentration (x)-temperature (T)-pressure (P) phase diagram of the system is characterized by a transition from an AF to a FE phase along with the appearance of some mixed regions upon changing concentration. Depending on concentration, one or two relaxation processes appear in the low-temperature region of the phase diagram. Measurement of the hysteresis loops and the current curves have been carried out along the (x - T - P)-phase diagram of this system. Multiple loops have been observed in various regions of the phase diagram. The correlation of the different contributions of the polarization and the temperature behavior of their critical fields with the main features of the temperature- and frequency-dependent dielectric constant enables clarification of the rich phase diagram obtained in this mixed compound in terms of the ferro- and/or antiferroelectric interactions.

DOI: [10.1103/PhysRevB.73.174118](https://doi.org/10.1103/PhysRevB.73.174118)

PACS number(s): 77.80.Dj, 77.80.Bh, 77.22.Gm

I. INTRODUCTION

Betaine arsenate [$(\text{CH}_3)_3\text{NCH}_2\text{COO}\cdot\text{H}_3\text{AsO}_4$ (BA), ferroelectric (FE)] and betaine phosphate [$(\text{CH}_3)_3\text{NCH}_2\text{COO}\cdot\text{H}_3\text{PO}_4$ (BP), antiferroelectric (AF)] are structurally very closely related and mixed crystals are formed in the ratio $\text{BA}_x\text{BP}_{1-x}$, with $0 \leq x \leq 1$. The (x , T)-phase diagram of $\text{BA}_x\text{BP}_{1-x}$ (Refs. 1–5) shows a variety of mixed regions and a glassy phase has been proposed for the intermediate concentration region. Although the phase diagram of the mixed $\text{BA}_x\text{BP}_{1-x}$ crystal system at low temperature shows dielectric dispersion due to several relaxation processes, typical features of the dipole glasses, such as the $\text{Rb}_x(\text{NH}_4)_{1-x}\text{H}_2\text{PO}_4$ (Ref. 6)-mixed system, are not seen. Furthermore, the nature of the different mixed-phase regions, transitions, and relaxations of the phase diagram seen in temperature and frequency dielectric function measurements are still not explained in a satisfactory manner from structural^{7,8} and spectroscopic data.⁵

The crystal structures of both BP (Ref. 9) and BA (Ref. 10) show the existence of quasi-one-dimensional chains of arsenate or phosphate tetrahedra, interconnected by hydrogen bonds. One betaine molecule is attached to each tetrahedron by two H bonds via the carboxyl groups, which differ in strength in the case of BP, but have approximately equal strength in BA. As a consequence, the deformations of the tetrahedra are subtly different in both compounds, resulting in a slightly different steric behavior. The length d_{H} of the H bonds connecting the tetrahedra, on the other hand, are almost identical in both compounds and d_{H} lies within the narrow region, where double-minimum potentials are to be expected for H bonds. The single chains in both BA and BP

are ferroelectrically ordered, however, the interchain interaction is slightly different for both crystals, which gives rise to the FE order of BA and the AF order in BP. Also BP and BA are not isostructural with each other at room temperature.^{9,10} BP undergoes a phase transition at 365 K from a paraelectric [$\text{P}2_1/\text{m}(\text{Z}=2)$] to an antiferrodistortive [$\text{P}2_1/\text{c}(\text{Z}=4)$] phase and a further isostructural transition into an AF phase at $T=86$ K, without doubling of the unit cell; for $T < 81$ K BP is AF [$\text{P}2_1/\text{c}(\text{Z}=8)$],^{9,11} while BA undergoes a phase transition from a paraelectric [$\text{P}c\text{nm}(\text{Z}=4)$] high-temperature phase to a ferroelastic [$\text{P}2_1/\text{n}(\text{Z}=4)$] one at 411 K, and a further transition into a FE [$\text{P}c(\text{Z}=4)$] phase at $T=119$ K.^{10,12}

From dielectric measurements, Raman and far-infrared spectroscopy,^{1–5} the concentration-temperature diagram (x , T) diagram^{1,2,4} was divided into four different regions, as indicated by the anomalies in $\epsilon'(T)$ and $\tan \delta(T)$ [i.e., $\epsilon''(T)$], which are as follows:

(a) *BP region* ($0 < x < 0.15$). The behavior is similar to that in pure BP, i.e., a phase transition at $T_{c2}=86$ K, ($x=0$) into an AF phase and a lower temperature anomaly at $T_d \approx 60$ K, ($x=0$) in $\tan \delta(T)$.

(b) *Intermediate Region A* ($0.15 < x < 0.50$). Characterized by two anomalies in $\epsilon'(T)$ ($T_{c2,a}$ and $T_{c2,b}$) and lower-temperature relaxations indicated by anomalies in $\tan \delta(T)$ ($T_{d,a}$ and $T_{d,b}$).

(c) *Intermediate Region B* ($0.50 < x < 0.80$). The double peak structure in $\epsilon'(T)$ disappears in favor of a single relatively broad anomaly. The same occurs in the behavior of $\tan \delta(T)$ at slightly higher concentrations. The double peak structure is recovered by applying external hydrostatic pressure.

(d) *BA region* ($x > 0.80$). There is no longer a transition

into an AF-type phase but into a FE one. The behavior in $\varepsilon'(T)$ and $\tan \delta(T)$ is similar to that in BA.

From a theoretical point of view, the quasi-one-dimensional Ising model has been applied to explain the behavior of the dielectric constant in the paraelectric phase,^{1,2} and dimensionality crossover from one to three dimensions by lowering temperature has been reported.¹³ The relaxational processes have been described in terms of “complex” and “simple” relaxations based on calculations of the activation entropies.^{4,14} The nature of the relaxations was discussed in terms of dipole-dipole and dipole-lattice interactions. Despite these efforts, the origin of the different transitions and relaxation processes is still unclear and x-ray diffraction studies reveal that the peculiar behavior of the mixed crystals cannot be explained from the structural point of view.^{7,8} On the other hand, Raman and Fourier transform infrared studies led to the conclusion that the FE or AF character of the ordered phase is related to the number of degrees of freedom of the AsO_4 and PO_4 tetrahedra.⁵ In the same way, these units determine the type and the modes triggering the phase transitions for each concentration.⁵ The latter seem to occur together with the participation of the betaine molecule, especially significant are the methyl and butyl groups. To summarize, the $\text{BA}_x\text{BP}_{1-x}$ system exhibits a (x, T) -phase diagram in which the transition from an AF to a FE phase can be observed with a concentration-dependent appearance of some mixed regions. At low temperatures, several relaxations have been observed. Despite the definition of the different regions from the anomalies of the dielectric function and the Raman and infrared spectra, the true nature of the dipolar ordering within the different regions of the phase diagram can only be achieved by measurement of the dielectric hysteresis loops.

In this paper, the measurements of the dielectric hysteresis and the current curves along the whole (x, T, P) -phase diagram will be reported and discussed. Measurements of the dielectric hysteresis loops have been previously reported for pure BA,^{15,16} BP,^{16,17} and deuterated BA.¹⁸ In deuterated BA, the transition with deuteration from single- to double-hysteresis loops, i.e., from FE to AF behavior, has been detected. Within the mixed crystals, measurements of the AF hysteresis loops have been only reported for $x=0.1$ (Ref. 19) and $x=0.73$.²⁰ Here, a detailed account of the dielectric hysteresis loops and current curves measurements along the (x, T, P) -phase diagram are presented. In this way, the ferroelectric order of the different phases is stated. Further, the correlation of the temperature dependence of the critical fields with the features observed in the measurements of the dielectric constant clarifies the origin and nature of the different phases of the phase diagram.

II. EXPERIMENT

The crystals were grown by controlled evaporation from aqueous solutions, and their concentrations were subsequently analyzed by means of ultraviolet spectroscopy and density methods to an accuracy of about 3%. Samples in the shape of thin slices ($d < 0.5$ mm) were oriented perpendicularly to the polar axis, and vacuum-deposited aluminium or

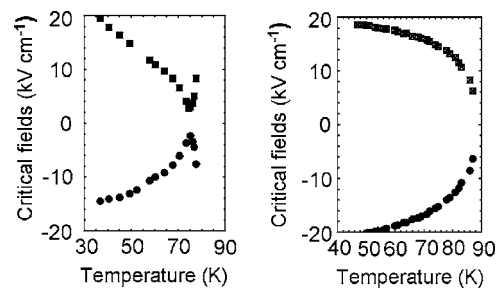


FIG. 1. Comparison of the critical fields of several samples in the AF region of the (x, T) -phase diagram. Left $x=0.00$, right $x=0.73$. The measurements were performed at a frequency of $\nu=10$ Hz and at normal pressure.

gold films served as electrodes. The temperature (23–300 K) and hydrostatic pressure ($p < 500$ MPa) dependence of the dielectric hysteresis loops and the current curves (derivatives of the hysteresis loops) were carried out at several frequencies with a home-built hysteresis bridge based on operational amplifiers and a dc high-voltage amplifier.²⁰ The charge current has, as compared to the polarization, the advantage of directly indicating the number of dipole reorientation processes for a certain electric field. It is therefore more sensitive for elucidating the changes occurring in the dipolar system. The maximum voltage applied to the sample was experimentally limited to 1000 V and the frequencies used were 0.1, 1, 10, and 100 Hz. The investigated concentrations were $x=0.00$,¹⁹ 0.24, 0.62, 0.73,²⁰ 0.94, and 1.00.¹⁹ Experiments under hydrostatic pressure were performed in a home-built cryostat and high-pressure chamber.²¹ Helium was used as pressure-transmitting medium. The pressure could be changed between atmospheric pressure and 500 MPa with an absolute uncertainty of ± 7 MPa.

III. EXPERIMENTAL RESULTS

Dielectric hysteresis and current curves for samples in each region of the phase diagram were measured by changing temperature, frequency, and hydrostatic pressure.

A. BP-region ($0 < x < 0.15$)

The measurements of the hysteresis loops and the current curves¹⁹ indicate that the transition into the AF phase occurs in two steps (Fig. 1, left). At T_{c2} , the transition into the AF phase occurs, but the critical field, at which the induced AF-to-FE transition takes place, is destabilized with decreasing temperature. At $\sim T_{c2} - 2.5$ K, the stabilization of the AF phase with decreasing temperature begins. On the other hand, the low-temperature anomaly at T_d coincides with the point at which the AF loops begin to open and a frequency dependence of the coercive field is detected. In this process, the stability limit of the induced FE phase increases more strongly than that of the AF phase. Increasing pressure induces a linear shift of the transition to lower temperatures.

B. Intermediate Regions A ($0.15 < x < 0.50$) and B ($0.50 < x < 0.80$)

1. Intermediate Region A

The measurements of the dielectric hysteresis for the sample with $x=0.24$ (Fig. 2) shows a transition at $T_{c2,a}$ into a

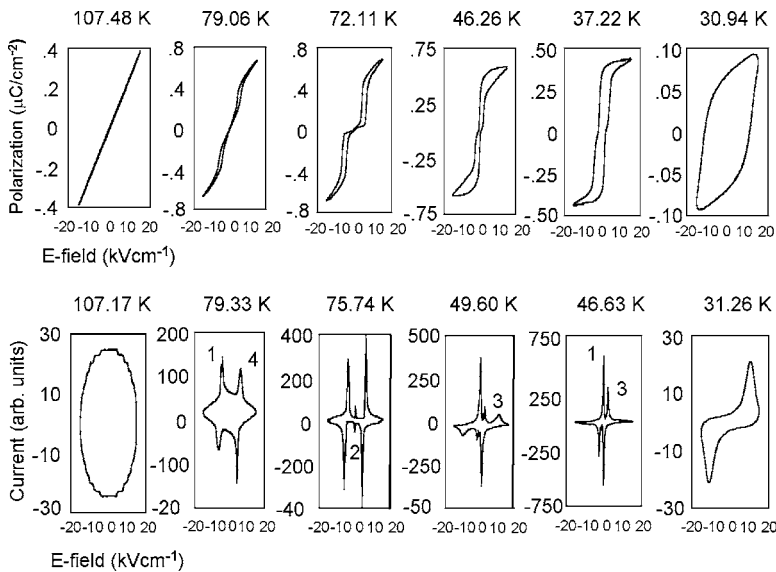


FIG. 2. (a) Typical hysteresis loops (above) and current curves (below) for $BA_{0.24}BP_{0.76}$ at $p \sim 50$ MPa in the different regions of the anomaly diagram. Measurements performed at $\nu = 10$ Hz.

nonpolar or AF phase. This phase is continuously destabilized (Fig. 3) down to $T_{c2,b}$; at this temperature, a FE component (2 in Fig. 3) and the stabilization of the AF components indicate the transition into a pseudo-antiferroelectric AF' phase, which is related to the onset of the dispersion and the increase in $\epsilon''(T)$.^{2,4} This process is apparently first-order with a jump in the extrapolated polarization from $0.3 \mu C cm^{-2}$ to $0.4 \mu C cm^{-2}$ at the transition point. Upon decreasing the temperature, the critical fields of the double hysteresis loops show increasing values for the FE and the AF critical fields. The FE phase develops a second component (3 in Fig. 3). Around $T = 52$ K, this double peak structure in the FE phase disappears. At 5 K below, the AF stability limit passes through $0 kV cm^{-1}$ and the polarization curves almost show a FE shape. Both remaining components strongly shift to higher fields at $T \sim T_{d,b}$. It should be noted that it is not possible to resolve the curves in our experimental window (Figs. 2 and 3). The critical fields increase linearly with increasing pressure, whereas the transition shifts to lower temperatures. The shape of the curves does not change with pressure. Therefore, there are several components contributing to the polarization; at least two competing interactions, and a strong destabilization of the AF' phase which disappears giving rise to a strong increase in the coercive field.

2. Intermediate Region B

Because of the differences in the dielectric behavior between the samples within this region (especially in the lower-

temperature region), we have investigated two samples by means of hysteresis loop and current curves measurements.

(1) The first sample is $BA_{0.62}BP_{0.38}$. In this case the curves show clear pressure dependence. At $T_{c2,a}$, the system undergoes a transition into an AF phase. This phase is stabilized very quickly with decreasing temperatures and the critical field of the induced FE phase goes beyond our experimental window of $\sim 30 kV cm^{-1}$ (Number 6 in Figs. 4 and 5). A second AF component appears some degrees below—4.2 K at 10 MPa, 10.7 K at 50 MPa, 16.2 K at 200 MPa—with lower critical fields (internal loops) (Figs. 4 and 5). This is a transition at $T_{c2,b}$ into a pseudo-AF phase, in which two different AF orders coexist. This anomaly cannot be observed in the dielectric measurements at low pressure^{2,4} because of the narrow temperature range between the two transitions. By increasing pressures, the shift to lower temperatures of $T_{c2,b}$ is larger than the shift of $T_{c2,a}$ which allows for a better definition of the anomaly in the dielectric function.^{2,4} At lower pressures, both AF components shift to higher fields with decreasing temperatures. A FE component arises because of the destabilization of the AF stability limit (zero-field crossing of the coercive field) of the lower field AF component (Fig. 5). This crossing coincides with a small hump in T_d .^{2,4} A new component in the polarization tends to stabilize the AF structure. This process is evidence for the existence of interactions of different signs and it also shows a strong frequency dependence. At higher pressures, the FE component is manifest in a different form, it does not appear from the existing AF structure, but due to a new dipolar

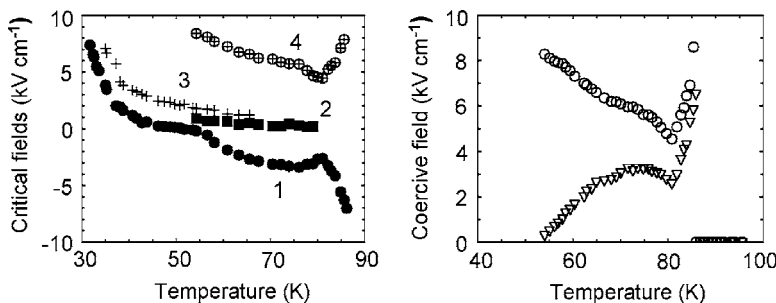


FIG. 3. Left, behavior of the critical fields taken from the peaks in the current curves of the $x = 0.24$ sample. The numbers correspond to the peaks in Fig. 2. Right, behavior of the coercive field taken from the hysteresis loops. Pressure ~ 10 MPa. The same behavior is observed at all pressures.

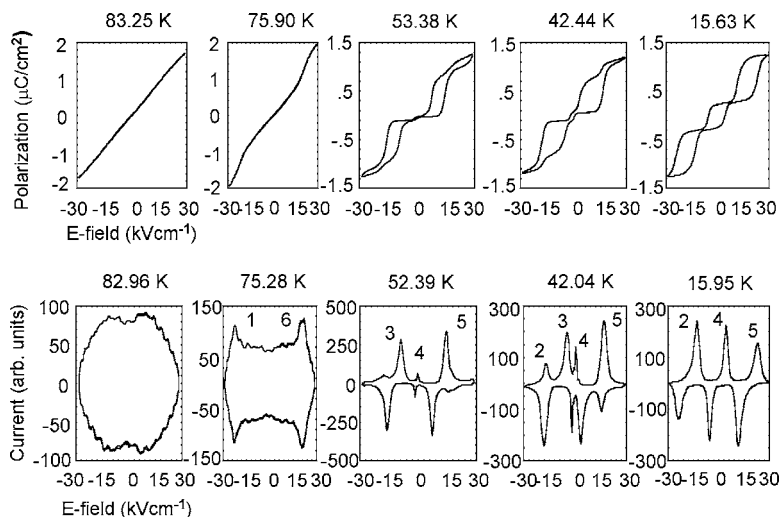


FIG. 4. (a) Typical hysteresis loops (above) and current curves (below) for $BA_{0.62}BP_{0.38}$ at $p \sim 50$ MPa in the different regions of the anomaly diagram. Measurements performed at $\nu = 10$ Hz.

contribution (Fig. 4). This component merges together with the AF component by its zero-field crossing. An uncompensated AF structure should remain, but again a new higher-field temperature-independent dipolar contribution tends to maintain the equilibrium in the secondary AF order. This combination of facts gives rise, in both cases, to three hysteresis loops at low temperature. At higher pressures, the two AF and the FE contributions (in this case very small) remain stable. The FE component vanishes which coincides with the anomaly at T_d (i.e., T_i), which is much stronger than at low pressures,^{2,4} which gives a double-hysteresis loop at low temperature.

(2) The second sample is $BA_{0.73}BP_{0.27}$. The behavior in this sample²⁰ is similar in respect to the existence of several contributions to the polarization, the complicated hysteresis loops, and the strong changes under external pressure. At $T_{c2,a}$, a transition into an AF-ordered phase occurs at normal pressure. The behavior of the critical fields Fig. 1, right, shows no special features. By increasing pressure in the region where the lower temperature anomaly in $\epsilon'(T)$ appears,^{2,4} the AF hysteresis loops split into at least two AF loops indicating two different dipolar systems.²⁰ Upon decreasing the temperature, the widths of the loops grow and those at low fields finally merge near 40 K to form a field-induced low-temperature FE phase, while the AF loop at higher-field strength persists.

3. BA region ($x > 0.80$)

The measurements of the hysteresis loops and especially those of the current curves¹⁹ show, that in the pure BA

($BA_{1.00}BP_{0.00}$) sample, the contribution of two components to the spontaneous polarization in an intermediate-temperature region inside the FE phase. Within the transition in the FE phase, we observe the typical peak in the current curves corresponding to an FE phase. At lower temperatures, this peak splits into two maxima coinciding approximately with the first maximum in $\tan \delta(T)$ [i.e., $\epsilon''(T)$].^{2,4} At lower temperatures, the two peaks merge again into a single one, and the coercive field becomes frequency dependent and increases strongly coinciding with the second anomaly in $\epsilon''(T)$. Below this, its height decreases strongly down to almost zero, i.e., the increase on the coercive field coincides with the definite freezing of the system. The relation between the splitting and merging of the different contributions to the polarization and the strong dissipations is obvious and they can be considered as the origin of the freezing process in this pure compound. Furthermore, at lower frequencies, three contributions to the current curves have been detected, which is evidence of the slow processes contributing to the properties of this phase.

The behavior of the hysteresis loops in the $BA_{0.94}BP_{0.06}$ sample is similar to the ones in pure BA.¹⁹ The main difference is that in this case the current curves show only the single peak typical for the FE state, i.e., there only appears to be one contribution to the polarization. We also observe a stabilization of the pure FE character due to the impurities. As in pure BA, the abrupt decrease in $\tan \delta(T)$ coincides with the strong (and frequency-dependent) increase in E_c (see Fig. 6). Thus, a freezing of the domain structure takes place at lower temperatures. The value of P_s is $2.7 \mu C cm^{-2}$, $0.3 \mu C cm^{-2}$ lower than for BA due to the BP AF impurities.

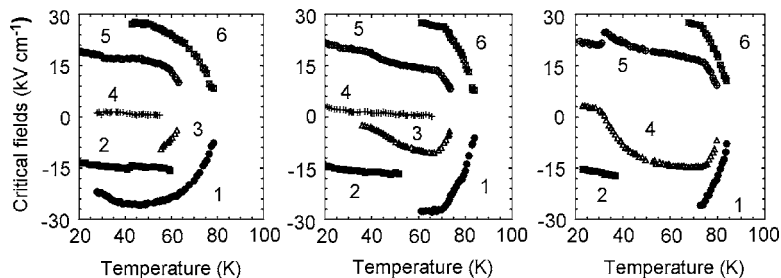


FIG. 5. Behavior of the critical fields taken from the peaks in the current curves for $BA_{0.62}BP_{0.38}$ at several pressures: from left to right, $p \sim 200, 50,$ and 10 MPa. The numbers correspond to the peaks in Fig. 4. Measurements performed at $\nu = 10$ Hz.

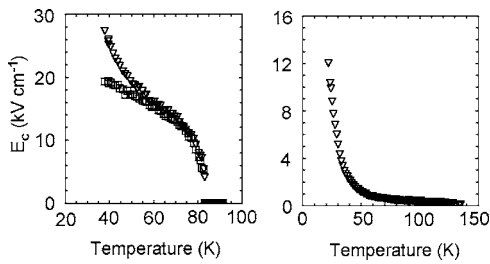


FIG. 6. Temperature behavior of the critical fields for two concentrations in the different regions of the phase diagram. Left, $x=0.00$; right, 1.00. The triangles represent the FE stability limit, whereas the squares represent the AF stability limit.

IV. DISCUSSION

A. Dipolar order along the (x, T, P) —phase diagram

The measurement of the hysteresis loops and the current curves have shown the evolution of the different components of the polarization and their values in the different regions of the phase diagram.

(1) For pure BP (Fig. 1), the transition into the AF seems to occur in two steps; the first, a transition into a nonpolar or AF phase occurs. This phase is destabilized at lower temperatures (decrease of the critical field) until the transition into the AF phase occurs, which is stabilized by lowering the temperature. Typical AF behavior has been observed down to the lowest temperature. Close to T_d , the critical field of the induced FE phase increases more strongly than the critical field of the AF phase, this induces an opening in the hysteresis loops.

(2) In the intermediate Region A (Fig. 3), the transition into the ordered phase occurs in the same way as in the previous region. However, in this region together with the beginning of the stabilization of the AF component, an FE component appears which coexists with the AF order and finally breaks the AF order at lower temperatures.

(3) The intermediate Region B is the most complex of all the four regions, and its behavior is concentration and pressure dependent. Whereas, at intermediate concentrations within this region (Fig. 5) the characteristic features are a coexistence of two AF contributions, with the low-energy component destabilizing with decreasing temperatures down to the development of a FE component, the higher concentrations (Fig. 1) within this region show a typical AF structure which freezes at lower temperatures. In this region, therefore, the crossover from one main AF order (BP type) to another ($x=0.73$ -type) occurs, with a coexistence of the two

at intermediate concentrations. This indicates that there are two systems of ordered units and we are tempted to assign these independent ordered units to the AsO_4 and PO_4 tetrahedra. At all concentrations, the effect of pressure produces an independent FE component which coexists with the AF orders.

(4) In the FE region of the phase diagram, a typical FE hysteresis loop is observed, but exhibiting several contributions that depend on frequency for pure BA and a stabilization of a pure FE structure is seen with increasing phosphate impurities. In all samples within this region, a strong and frequency-dependent increase of the coercive field coinciding with the drop in $\tan \delta(T)$ for lower temperatures is observed, and this is indicative for the definite freezing of the system (Fig. 6).

The evolution of the polarization with concentration is represented in Fig. 7 for several electric fields at different temperatures. A continuous decrease in the polarization from pure BA down to the intermediate Region B and a stabilization in the other two regions is observed.

From these results and previous dielectric data,^{2,4} the phase (x, T) diagram can be drawn at several pressures, showing the evolution of the different regions and their stability against the external pressure Fig. 8. The whole phase diagram is shifted toward lower temperatures by increasing external pressure, but not homogeneously. Whereas the AF phase is stabilized (i.e., the AF regions increase at the expense of the AF' and AF''), the FE phase almost disappears under an increase in pressure. However, the pseudo-AF phase survives in a smaller temperature range, whereas the pseudo-FE occupies a larger one. A crossover of the two low-temperature relaxation processes occurs at $x \approx 0.60$, and thus changes the character of the low-temperature region. The main behavior of the low-temperature relaxation was studied in Ref. 4, and in order to explain the main features of the different regions and its behavior under external pressure, the interplay of two order parameters and the variations on their free energy and relative coupling have to be taken into account.

It is interesting to compare the effect of external pressure with the effect of increasing concentration of impurities, starting with the pure materials up to $x \approx 50\%$. Whereas for pure BP the arsenate, the impurities induce a negative chemical pressure (the opposite effect as the hydrostatic pressure), i.e., an expansion of the lattice; for pure BA, the increase of phosphate impurities represents the same effect as hydrostatic pressure. It should, however, be noted that the volume of the unit cell of BA exceeds the volume of BP at 300 K.^{9,10}

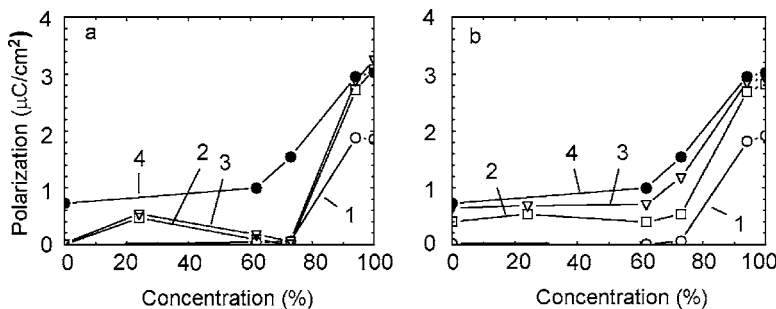


FIG. 7. Value of the polarization for several electric fields [2 (1), 10 (2), 15 (3), and 20 (4) $kV\ cm^{-1}$] at a temperature $T_{c2}=40\ K$ (a) and $T_{c2}=5\ K$ (b) for concentrations in the different regions of the (x, T) -phase diagram $\nu=10\ Hz$. $p \sim 50\ MPa$. Solid lines are drawn to guide the eyes.

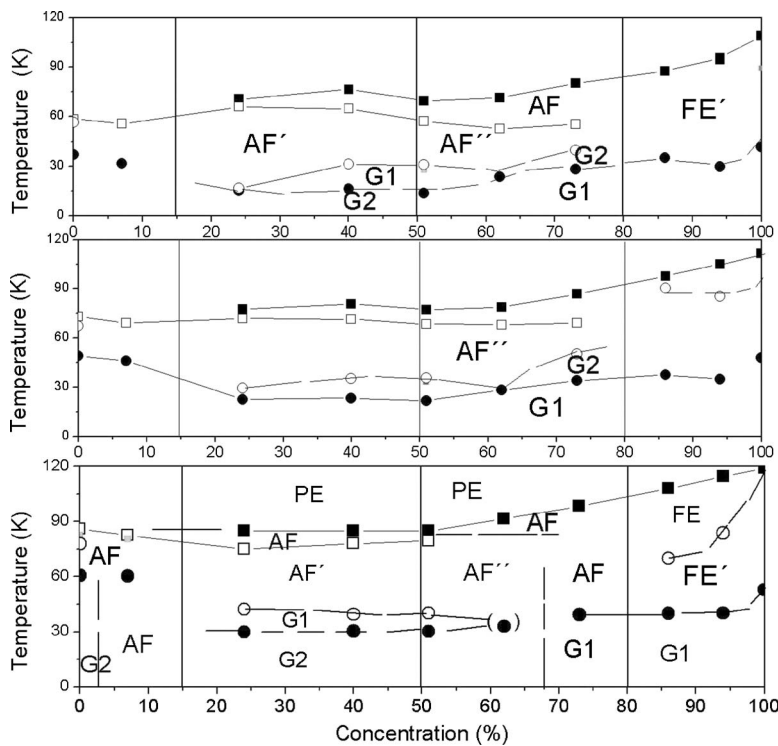


FIG. 8. (x, T) diagram at several pressures; 0, 200, and 400 MPa from bottom to top. The evolution of the different regions and their stability against the external pressure can be observed. The points are extrapolations from the linear fits in the (p, T) phase diagrams, obtained from the dielectric results for the different samples at $\nu = 100$ kHz (Refs. 1, 2, and 4) and from the measurements of the hysteresis loops. Black and open squares, anomalies in $\epsilon'(T)$, black and open circles, anomalies in $\tan \delta(T)$ [i.e., $\epsilon''(T)$]. The brackets in $\tan \delta(T)$ indicate that the anomalies much smaller than the others, so that the corresponding anomaly in $\epsilon''(T)$ could not be observed. From the hysteresis measurements, the various types of order are indicated. AF, antiferroelectric, AF', coexistence FE (ferroelectric) and AF components, AF'', coexistence of two AF components, G, Freezing process, G1, Vogel-Fulcher, (VF), i.e., collective relaxation, G2: Arrhenius, (A), i.e., single-ion relaxation, FE', FE with domain freezing process. Solid lines are drawn to guide the eyes.

B. Theoretical considerations

The experiments using $\text{BA}_x\text{BP}_{1-x}$ at intermediate concentrations show the existence of two different instabilities at the transition into the ordered phase. Furthermore, the experiments in the pure compounds suggest that we are not dealing with a conventional AF or FE phase transition. Moreover, the results obtained for $\text{BA}_{0.94}\text{BP}_{0.06}$ and BA suggest that two order parameters, a FE and a structural one, could play a role in the transition process. The behavior of systems with two order parameters has been studied in several papers,^{22,23} since then the Kittel model²⁴ has been transformed into a form explicitly containing those two instabilities.^{25,26} In Refs. 27 and 28, a detailed analysis of the simplest phenomenological model with FE and structural instabilities was presented, with the Kittel model as a special case. The dielectric response, the phase diagrams in the presence of an electric field, and the behavior of the hysteresis loops were theoretically investigated from the following free-energy expansion,

$$F = \frac{1}{2}\alpha_1\eta^2 + \frac{1}{4}\beta_1\eta^4 + \frac{1}{2}\alpha_2P^2 + \frac{1}{4}\beta_2\eta^4 + \frac{1}{2}\gamma\eta^2P^2 - PE \quad (1)$$

where η is the structural order parameter, P is the polarization, E is the macroscopic electric field parallel to the polar axis, $\alpha_1 = \lambda_1(T - T_{c\eta})$, $\alpha_2 = \lambda_2(T - T_{cp})$, and β_1 , β_2 , and γ are positive. $\gamma \geq 0$ corresponds to the suppression of the FE ordering in the presence of a nonpolar order parameter. The sign of γ is of primary importance for the behavior of the system. For $\gamma \leq 0$, the system may reveal, for example, a trigger-type phase transition.²⁹ $T_{c\eta} = T_{c2}$ is associated with the AF transition temperature.

The model shows six qualitatively different types of behavior characterized by two independent parameters Δ and Φ ,

$$\Delta = \left(\frac{\lambda_1}{\lambda_2}\right)\left(\frac{\beta_2}{\beta_1}\right)^{1/2} \quad \text{and} \quad \Phi = \gamma(\beta_1\beta_2)^{-1/2} \quad (2)$$

The parameter Δ reflects the difference in the temperature dependencies between the energies for the nonpolar ordered state ($P=0, \eta \neq 0$) and polar state ($P \neq 0, \eta=0$) and the parameter Φ determines the coupling between the order parameters. There are several regions in the (Δ, Φ) plane which describe a different behavior. These regions were called U, T, S, I, W1, and W2 (Refs. 27 and 28), and differ in the form and temperature behavior of the dielectric anomaly at the structural phase transition and the type of hysteresis loop observed. With respect to the presence and type of double hysteresis loops, the model is divided into regions with no loops (U, W1, and W2), double hysteresis loops diverging on cooling (T) and double hysteresis loops converging on cooling (S and T). The presence of a FE hysteresis loops was found in the regions S, I, W1, and W2, but was absence in the regions U and T.

The model was successfully applied to deuterated betaine arsenate (Ref. 28) over the complete concentration range. Comparing our measurements with the model, some striking similarities between the BP region and the T region, the intermediate region A and the S region, and the BA region and the W2 regions have been found, both in the behavior of $\epsilon'(T)$ and in the behavior of the critical fields. This can be seen by comparing the results obtained for the $\epsilon'(T)$ behavior⁴ for the different concentrations and Figs. 3 and 6 with the results from Refs. 27 and 28. Here, the BP region can be characterized by a transition sequence PE

$(\eta=0, P=0) \rightarrow \text{nonpolar}(\eta \neq 0, P=0)$, the intermediate region for a sequence $(\eta=0, P=0) \rightarrow \text{nonpolar}(\eta \neq 0, P=0) \rightarrow \text{polar}(\eta=0, P \neq 0)$ or $(\eta=0, P=0) \rightarrow \text{nonpolar}(\eta \neq 0, P=0) \rightarrow \text{mixed}(\eta \neq 0, P \neq 0)$, and the BA region by a sequence: $(\eta=0, P=0) \rightarrow \text{nonpolar}(\eta \neq 0, P=0) \rightarrow \text{mixed}(\eta \neq 0, P \neq 0)$. In this way, this model seems to explain the transition with concentration from an AF to a FE phase depending on the value of the two model parameters. It should be noted, however, that striking differences have also been found and a quantitative analysis of the phase behavior applying this model was not possible. To conclude, it seems clear that at least two order parameters are necessary to describe the system, but other contributions (e.g., for the possibility of first-order phase transitions) are required in order to account for its rich properties.

C. H Bonds versus AsO_4/PO_4 groups

In the BA-BP system, proton tunneling might play a role as the lengths of the H-bonds in the pure compounds are found to be close to 2.5 Å, where a symmetrical double minimum potential can be expected. There is, however, no clear experimental evidence for this effect. A nonlinear shift with increasing pressure in the $\epsilon'(T)$ anomalies between $x=51\%$ and 100% could not be explained using the possibility of proton tunneling (nonphysical fit parameters).²¹ The interaction between the different dipolar contributions observed in the hysteresis loops and current curves, which are responsible for the two different anomalies and/or the plateau in $\epsilon'(T)$ in these samples seems to be the only way to explain this effect.

Furthermore, there is some evidence for the important role of the proton degrees of freedom in BA and BP.^{15,17} This is especially true in the case of BPI and the BP:BPI(x) system.^{30,31} The distortion of the tetrahedra^{32,33} was shown to contribute to the polarization, and this was also proposed as a mechanism responsible for the ordered phase, where only partial proton order was found. Raman results⁵ support the importance of the tetrahedra dynamics in the various phases, both with temperature and with concentration. The experiments under increasing hydrostatic pressure and analysis with the quasi-1D Ising model point toward the importance of the interactions in the plane perpendicular to the polar axis.²⁰ The striking differences found in the BP/BPI

system^{34,35} can also be explained by making the tetrahedra and the bonds with the betaine molecule responsible for the dipolar behavior. These are the main differences between the two mixed systems and the three pure compounds.

The dielectric function ϵ'_y (field along the spontaneous sublattice polarization) has been measured for pure BP (Ref. 1) and found to depend on the uniaxial pressure applied along the monoclinic axis y and x' , z' (directions in the monoclinic plane without shear strain). A shift of the transition temperature at T_{C2} only occurs if pressure is applied in the y direction. Here, the slope $(dT_{C2}/dp_y)_{\text{BP}}$ amounts to -0.021 K/MPa, which is about one-third of the slope for hydrostatic compression. A compression along the y axis results in a shortening of the H bonds connecting the phosphate tetrahedra, i.e., in a destabilization of the low-temperature ordered phase. These bonds also contribute to the AF or FE character of the ordered phase.^{20,21}

The experimental results⁴ show that the local freezing of the protons in their double-well potential occurs at lower temperatures than the transition into the ordered phase, that it is independent of the dipoles formed at these transitions and corresponds to a relaxation process fitted with an Arrhenius law. However, the freezing process, which follows the Vogel-Fulcher law, is obviously related to the dipolar structure from the transition into the ordered phase, as shown by the temperature behavior of the critical fields of the hysteresis loops. These can be associated with the tetrahedra degrees of freedom.⁵

V. CONCLUSION

The temperature-concentration phase diagram of the $\text{BA}_x\text{BP}_{1-x}$ mixed crystal system and its behavior under external hydrostatic pressure has been discussed and analyzed in terms of measurements of the dielectric hysteresis and current curves. The ferroelectric, antiferroelectric, or mixed character of different regions of the phase diagram have been identified in the light of the complex hysteresis loops. Several ferro- and antiferroelectric components compete along the temperature-concentration phase diagram and are responsible for the different behaviors observed in previous dielectric measurements. The interplay of two order parameters, one polar and the other nonpolar, seem to be behind the complex behavior exhibited by this system

¹S. Lanceros-Méndez, G. Schaack, and A. Klöpperpieper, *Ferroelectrics*, Frontiers in Science and Technology-Science and Technology of Ferroelectrics Vol. 2 (Stefan University Press, La Jolla, California, 2001), ISBN: 1889545295.

²S. Lanceros-Méndez and G. Schaack, *Ferroelectrics* **226**, 107 (1999); S. Lanceros-Méndez and G. Schaack, *J. Korean Phys. Soc.* **32**, S850 (1998).

³M. Maeda, *Ferroelectrics* **96**, 269 (1989); M. Maeda and I. Suzuki, *ibid.* **108**, 351 (1990); S. Hayase, T. Koshihara, H. Terauchi, M. Maeda, and I. Suzuki, *ibid.* **96**, 221 (1989).

⁴J. F. Mano and S. Lanceros-Mendez, *J. Appl. Phys.* **89**, 1844 (2001).

⁵S. Lanceros-Mendez, H. Ebert, G. Schaack, and A. Klöpperpieper, *Phys. Rev. B* **67**, 014109 (2003).

⁶U. T. Hochli, K. Knorr, and A. Loidl, *Adv. Phys.* **51**, 589 (2002).

⁷T. Yoshida, H. Mashiyama, and T. Mochida, *J. Korean Phys. Soc.* **35**, 1409 (1999).

⁸T. Yoshida, H. Mashiyama, and T. Mochida, *J. Phys. Soc. Jpn.* **70**, 1598 (2001).

⁹W. Schildkamp and J. Spilker, *Z. Kristallogr.* **168**, 159 (1984).

- ¹⁰W. Schildkamp, J. Spilker, and G. Schäfer, *Z. Kristallogr.* **168**, 187 (1984).
- ¹¹T. Yoshida, H. Mashiyama, and T. Mochida, *J. Phys. Soc. Jpn.* **70**, 569 (2001).
- ¹²H. J. Rother, J. Albers, A. Klöpperpieper, and H. E. Müser, *Jpn. J. Appl. Phys., Part 1* **24**, Suppl. 24–2, 384 (1985).
- ¹³Y.-H. Kim, B.-G. Kim, J.-J. Kim, T. Mochida, and S. Miyajima, *J. Phys.: Condens. Matter* **8**, 6095 (1996).
- ¹⁴S. Lanceros-Méndez, J. F. Mano, and J. A. Mendes, *Ferroelectrics* **270**, 1457 (2002).
- ¹⁵H. E. Müser and U. E. Schell, *Ferroelectrics* **55**, 279 (1984); U. Schell, *Ferroelectrics* **4**, 123 (1985).
- ¹⁶S. Lanceros-Méndez, G. Schaack, M. Köhler, and A. Klöpperpieper, *Ferroelectrics* **176**, 73 (1996).
- ¹⁷J. Albers, A. Klöpperpieper, and H. J. Rother, *Phys. Status Solidi A* **74**, 553 (1982); I. Suzuki, N. Otha, and M. Maeda, *Ferroelectrics* **96**, 485 (1989).
- ¹⁸E. V. Balashova, V. V. Lemanov, A. B. Sherman, and S. Shmuradov, *Ferroelectrics* **159**, 1 (1994).
- ¹⁹Y.-H. Kim and J.-J. Kim, *Phys. Rev. B* **55**, R11933 (1997).
- ²⁰M. Manger, S. Lanceros-Mendez, G. Schaack, and A. Köpperpieper, *J. Phys.: Condens. Matter* **8**, 4617 (1996).
- ²¹S. Lanceros-Mendez, Ph.D. thesis, Universität Würzburg, 1996.
- ²²V. E. Yurkevich, B. N. Roloy, and H. E. Stanley, *Ferroelectrics* **16**, 61 (1977).
- ²³Yu. M. Gufan and E. S. Larin, *Fiz. Tverd. Tela (Leningrad)* **22**, 463 (1980).
- ²⁴Ch. Kittel, *Phys. Rev.* **82**, 729 (1951).
- ²⁵L. E. Cross, *Philos. Mag.* **1**, 76 (1956).
- ²⁶K. Okada, *J. Phys. Soc. Jpn.* **27**, 420 (1969).
- ²⁷E. V. Balashova and A. K. Tagantsev, *Phys. Rev. B* **48**, 9979 (1993).
- ²⁸E. V. Balashova, V. V. Lemanov, A. K. Tagantsev, A. B. Sherman, and Sh. H. Shomuradov, *Phys. Rev. B* **51**, 8747 (1995).
- ²⁹B. A. Strukov, *Phase Transitions* **15**, 143 (1989).
- ³⁰H. Bauch, R. Böttcher, and G. Völkl, *Phys. Status Solidi B* **178**, K39 (1993); **179**, K41 (1993).
- ³¹P. Freude and D. Michel, *Phys. Status Solidi B* **195**, 297 (1996); P. Freude, D. Michel, J. Totz, and A. Klöpperpieper, *Ferroelectrics* **208**, 93 (1998).
- ³²G. Fischer, H. J. Brückner, A. Klöpperpieper, H. G. Unruh, and A. Levstik, *Z. Phys. B: Condens. Matter* **79**, 301 (1990).
- ³³K. H. Ehses and J. Spilker, *Ferroelektrizität 89*, Wissenschaftliche Beiträge Martin Luther Universität, Halle-Wittenberg, edited by G. Schmitt and A. Rost (Halle Saale, 1990).
- ³⁴H. Ries, R. Böhmer, I. Fehst, and A. Loidl, *Z. Phys. B: Condens. Matter* **99**, 401 (1996).
- ³⁵M. L. Santos, M. R. Chaves, A. Almeida, A. Klöpperpieper, H. E. Müser, and J. Albers, *Ferroelectr., Lett. Sect.* **15**, 17 (1993).